Fractal characteristics and damage evaluation of corroded beams under four-point bending tests based on acoustic emission techniques

Zheng, Yonglai; Wen, Yuan; Pan, Tanbo; Liu, Yongcheng; Zhou, Yujue; Li, Ruizhi; Zhou, Yubao

DOI
10.1016/j.measurement.2022.111792

Publication date
2022

Document Version
Final published version

Published in
Measurement: Journal of the International Measurement Confederation

Measurement 202 (2022) 111792

Contents lists available at ScienceDirect

Measurement

journal homepage: www.elsevier.com/locate/measurement

Fractal characteristics and damage evaluation of corroded beams under four-point bending tests based on acoustic emission techniques

Yonglai Zheng [a], Yuan Wen [a], Tanbo Pan [a,*], Yongcheng Liu [a], Yujue Zhou [a,b], Ruizhi Li [a], Yubao Zhou [c]

[a] Department of Hydraulic Engineering, Civil Engineering college, Tongji University, China
[b] Department of Civil Engineering, Sanming University, China
[c] Faculty of Civil Engineering and Geosciences, Delft Univerisity of Technology, Netherlands

ARTICLE INFO

Keywords:
Acoustic emission
Concrete fracture monitoring
Damage assessment
Fractal Characteristics
Steel corrosion

ABSTRACT

This study investigated the relationship between the acoustic emission (AE) signals parameter sequence fractal characteristics and the damage evolution information of corroded reinforced concrete (RC) beams under four-point bending. Strength deterioration behavior and AE data can be obtained by coupling the four-point bending test and the AE monitoring. The results show that AE ringing counts of corroded and uncorroded beams had prominent fractal characteristics. The fractal dimension values of corroded RC beams all showed a fluctuating rise to a peak and then a sharp drop before the failure. The damage index corresponding to the peak point decreases with the increase of corrosion degree. Fractal dimension peak point could be used as an early warning point for corroded RC beams' failure. Moreover, the AE fractal dimension analysis can effectively reflect the pattern of crack development, which have an important value for evaluating the process of corroded RC beams rupture.

1. Introduction

Corrosion of steel reinforcement is a worldwide issue that has an adverse effect on both the serviceability and durability of reinforced concrete structures [1–5]. Generally, reinforcement corrosion leads to severe deterioration, such as cracking and spalling of the concrete cover, owing to the corrosion products occupying two to six times more volume than the initial volume [6]. In particular, these deteriorations weakened the hoop restraint and reduced the bond behavior between the reinforcement and the concrete, which inevitably caused severe structural damage [7]. Therefore, it is necessary to quantitatively analyze and characterize the damage evolution to ensure the durability and safety of reinforced concrete (RC) structures.

Acoustic emission (AE) technique is a non-destructive testing technique, which provides an objective assessment of various damages to RC structures, such as cracks, honeycomb, and corrosion [8–12]. It uses AE sensors to passively capture elastic wave signals generated by material damage or deformed [9,13–15]. AE technique has the advantages of high sensitivity [16] and the ability to detect damage in real-time [17], making it an effective tool for monitoring the evolution damage of RC structures. Therefore, many researchers have carried out laboratory experiments from different aspects to investigate the AE characteristics of corroded RC members. Abouhussien et al. [18] assessed the bond behavior of corroded bars in reinforced concrete prism samples under pull-out tests using AE techniques. The results confirmed an excellent correlation between AE cumulative number of hits and AE signal strength parameters with the steel-to-concrete bond degradation because of corrosion. Abdelrahman et al. [19] established a relationship between cumulative AE energy and the degree of damage to RC beams and proposed an improved damage index to detect the yield point of corroded beams. Garhwal et al. [20] used local AE technique to evaluate the behavior and performance of corroded large-size reinforced concrete beams under bending loads. Kawasaki et al. [21] applied the AE technique to evaluate the seismic capacity of the specimens subjected to the influence of rebar corrosion and compared the relationship between mechanical properties and AE parameters. The AE technique is one of the methods used to study the failure patterns of RC structures.

In the last three decades, the fractal theory has received great attention as a tool for studying nonlinear systems, especially in mechanics and solid-state physics [22–26]. Mandelbrot has pointed out

* Corresponding author.
E-mail address: 1830149@tongji.edu.cn (T. Pan).

https://doi.org/10.1016/j.measurement.2022.111792
Received 9 May 2022; Received in revised form 13 August 2022; Accepted 19 August 2022
Available online 27 August 2022

that the complex geometry of fractal objects cannot be described by an integral dimension [27]. This phenomenon is usually expressed in terms of the statistical scaling laws of space or time domain, which is mainly manifested as the power-law behavior of real-world physical systems [28]. It indicates that fractals apply to objects in space or to fluctuations in time, with some form of self-similarity [29,30]. The magnitude of individual AE parameters (e.g., AE energy, AE ringing counts, etc.) exhibit a disorder in time. Therefore, fractal analysis of AE signals provided a useful way to characterize the damage evolution of specimens. Zha et al. [31] analyzed the damage development and temporal and spatial evolution of the AE parameters of rock under different loading modes. Results showed that the sequence of total AE events and AE counts under different loading modes was UCT (uniaxial compression tests) > DTT (direct tensile tests) > ITT (indirect tensile tests). Zhao et al. [32] explored the correlation between fractal characteristics associated with AE signals and mechanical damage in tantalum niobium tailings CPB materials with varying proportions. The findings indicated that the fractal dimension's amplitude is relatively concentrated, implying that it can correctly predict the failure of cement slurry backfill. Sun et al. [33] discussed the fractal characterization of coal rock damage stresses and AE signals, providing a quantitative guide to rock stability analysis in excavation projects.

For RC structural components, there are many studies that have characterized evolution characteristics using the fractal or multifractal analyses of the accompanying AE signals. Liu et al.[34] used the fractal method to study the evolution characteristics of concrete with different initial porosities under uniaxial cyclic loading conditions. The results show that the trends of AE energy and the correlation dimension of AE energy of concrete specimens with different initial porosity are basically the same with the loading process. Wu et al.[35] analyzed the fractal characteristics of AE parameters sequence of prestressed RC beams during the flexural failure. The results showed that the fractional decrease in the correlation dimension of the AE signal energy parameter implies the appearance of damage, which can be used for health monitoring and nondestructive testing of prestressed reinforced concrete beams. Wang et al. [36] proposed a model to reflect the damage degree of the RC beams structures. The results indicated that more severe damage would appear when the correlation dimension is stable after damage. Wang et al. [37] investigates the effect of steel fibers on the damage characteristics of concrete under uniaxial tension based on the fractal method. The results showed that the correlation dimension increased and then decreased with increasing stress level before the peak stress; the average correlation dimension increased with the increase of steel fibers. These results are valuable for enriching early warning of fracture of steel fiber reinforced concrete. However, few studies have focused on the fractal analysis of AE signals of RC structures with different corrosion damage. Therefore, quantitative multi-fractal analysis of AE parameters resulting from corroded beams fracturing experiments requires further study.

Using the AE technique, this present study aims to monitor the damage evolution in corroded RC beams. Laboratory experiments on four RC beams with different degrees of corrosion (0, 5%, 10%, 20%) under four-point bending tests are conducted to obtain AE data. First, the variation characteristics of AE ringing counts with loading were investigated and compared with the monitoring results of load–deflection curves. Next, a damage evolution model of corroded RC beams was proposed based on cumulative AE ringing counts. Subsequently, this study applied the fractal theory to analyze the AE characteristics of corroded RC beams subjected to four-point bending. This work improves the accuracy of early warning of fracture damage of corroded RC beams based on AE monitoring.

2. Experimental program

2.1. Materials and specimens

Four RC beams were manufactured with a width of 150 mm, a height of 200 mm, and a length of 1600 mm with an effective span of 1300 mm. Each beam was equipped with two longitudinal deformed steel rebars of 14 mm diameter in the tension region and two longitudinal deformed steel rebars of 8 mm in the compression region. Round steel rebars of 6 mm diameter were used as stirrups with a hoop spacing of 80 mm. The concrete cover was 25 mm. The contact position of the stirrups and longitudinal tensile steel rebars was covered with a layer of epoxy resin to prevent the corrosion of the stirrups. Fig. 1 shows the geometry and reinforcement details of RC beams.

All beams were cast with the in-situ mixed concrete having equivalent compressive strength. Table 1 shows the mixture proportions of concrete. The concrete compressive strength was 42.5 MPa (the standard deviation was 3.6 MPa) determined from three standard concrete prisms with dimensions of 150 × 150 × 300 mm after 28 days of normal curing. Tensile tests were performed on longitudinal deformed steel rebars for 14 M and 8 M and stirrups. The yield strength, ultimate strength, and elastic modulus longitudinal deformed steel rebars for 14 M were found to be 462.2 MPa (the standard deviation was 5.5 MPa), 615.7 MPa (the standard deviation was 16.2 MPa), and 200 GPa, respectively, as well as the corresponding material properties for the 8 mm deformed steel rebars were 408.9 MPa (the standard deviation was 4.5 MPa), 611.3 MPa (the standard deviation was 15.2 MPa), and 200 GPa respectively, and for the 6 mm round steel rebars were 352.7 MPa (the standard deviation was 3.7 MPa), 425.5 MPa(the standard deviation was 15.1 MPa), and 200 GPa respectively. Table 2 summarizes the properties of the material.

2.2. Accelerated steel corrosion tests

Fig. 2 shows the experimental setup of the accelerated corrosion tests. As shown there, the corrosion region was 1300 mm long between the two supports, and a customized water tank was fixed at the bottom of the RC beam. The water tank was filled with 5% NaCl solution to corrode the RC beams. The water tank with dimensions of 1300 × 230 × 180 mm was cut in the width direction with an 80 mm depth groove to fix the beam. The level of the solution is about 150 mm, which could keep the solution just submerging the tensile reinforcement of the RC beams. To ensure that the corrosion area inside RC beams contained sufficient NaCl solution, the RC beams need to be pre-soaked for seven days before accelerated corrosion tests. The test adopted the eTM-305F type adjustable regulated DC power supply, whose maximum output voltage is 30 V and maximum output current is 5A. During the accelerated corrosion process, the 14 mm longitudinal deformed steel rebars immersed in NaCl solution were connected to the positive electrode of the power supply as the anode of the electrochemical reaction, and a layer of wire mesh wrapped around the RC beams acted as a cathode connected to the negative terminal of the power supply[38]. It was noted that the target ampere density was set as 180 $\mu A/cm^2$ to simulate the corrosion in natural state and avoid the bond loss at the interface between steel bars and concrete[39]. The Faraday's law is used to calculate the theoretical mass loss of tensile reinforcement, as expressed in Eq. (1).

$$m_s = \frac{M \cdot i \cdot S_a \cdot T}{Z \cdot \mathrm{F}} \tag{1}$$

Where: m_s is the mass loss of the steel bar; M is the atomic weight of iron (56 g/mol); i is current density (A/cm^2); S_a is the area of the rebar (cm^2); T is the accelerated steel corrosion time (s); Z is the valence of the reacting electrode of the material (equal to 2); F is the Faraday's constant (96,500C/mol). The ratio of m_s and original mass of the steel bar can be used to determine the corrosion degree. As mentioned above, the

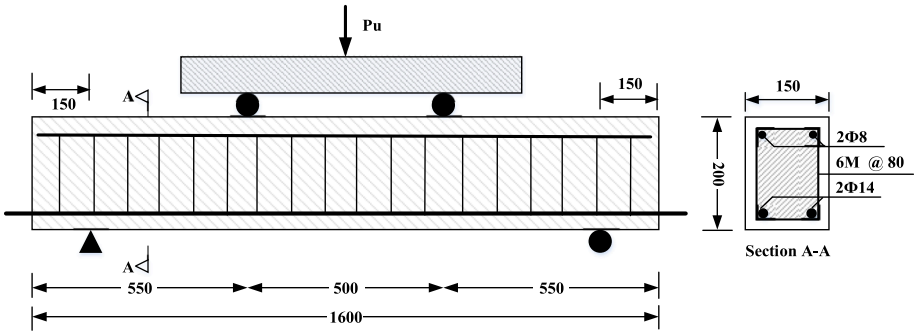

Fig. 1. Details of beam specimen (units are in mm).

Table 1
Concrete mixture proportions.

Concrete grade	Density (kg/m^3)	Fine aggregate /aggregate	Water/cement ratio	Specific weight(kg/m^3)		
				Cement	Fine aggregate	Coarse aggregate
C40	2374	0.45	0.6	383.3	792.3	968.4

Table 2
Material properties.

Materials	Yield strength	Ultimate strength	Compressive strength	Elastic modulus
Concrete	–	–	42.5 ± 3.6 MPa	–
D14	462.2 ± 5.5 MPa	615.7 ± 16.2 MPa	–	200 GPa
D8	408.9 ± 4.5 MPa	611.3 ± 15.2 MPa	–	200 GPa
R6	352.7 ± 3.7 MPa	425.5 ± 15.1 MPa	–	200 GPa

Note: D14 and D8 denote 14 mm and 8 mm deformed steel rebars; R6 denotes round steel rebars.

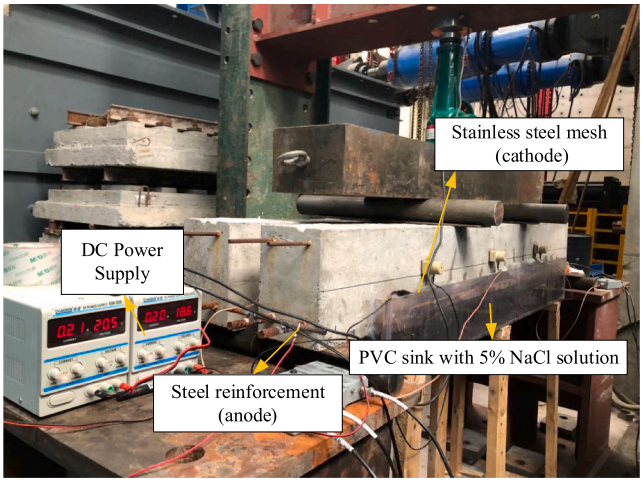

Fig. 2. Experimental setup of the accelerated corrosion process.

target corrosion degrees were taken as 5%, 10%, and 20% and the corresponding periods of accelerated steel corrosion were 25, 50, and 100 days respectively. C0 refers to a healthy control beam with no corrosion., while C5, C10, and C20 represent the beams with different degrees of corrosion (5%, 10%, 20%), respective.

2.3. Test setup and AE monitoring

All the tested beams were subjected to four-point bending test, as shown in Fig. 3. The concentrated load was applied to the tested RC beams by a 500 kN servo-hydraulic actuator at a rate of 1.0 mm/min, controlled by the MTS closed-loop system. The deflections at midpoint of beam and two loading points were monitored by linear variable displacement transducers (LVDTs).

A sixteen-channel PCI-2 AE System manufactured by the American Physical Acoustics Company (PAC) was adopted to detect and collect the AE signals within the collection area during the loading process. Five multi resonant VS45-H piezoelectric sensors were mounted on each specimen, as indicated in Fig. 4. The sensor surface was applied a coat with petroleum jelly to ensure coupled contact with the concrete surface [40]. The sensors had a frequency response range of 10–100 kHz. A threshold level of 40 dB was set to eradicate background noise interference. Since long-distance transmission causes a reduction in the signal-to-noise ratio of AE signals, the gain of the preamplifier was set to 40 dB to increase the signal strength. Prior to the AE monitoring tests, a pencil break (PLB) test should be carried out to check the sensitivity and coupling characteristics of the AE sensors.

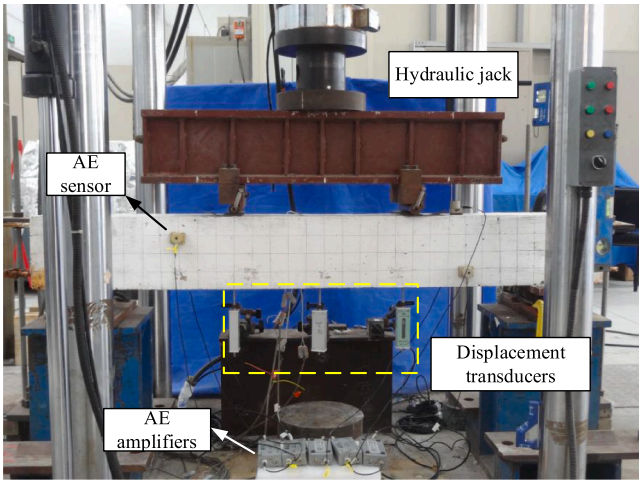

Fig. 3. Laboratory loading test of specimens.

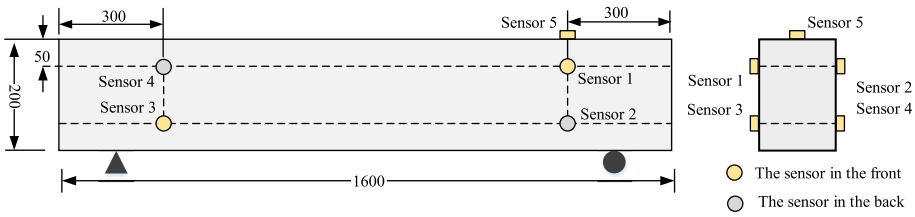

Fig. 4. The layout of AE sensors.

3. Fractal dimension analysis of AE of corroded beams

3.1. Calculation of correlation dimension

It has been shown that the AE signals can well reflect the occurrence and development of cracks in the RC beams. [41,42]The AE signals generated during the deformation and damage of RC beams have fractal characteristics. Moreover, an increase in the fractal dimension indicates that events are moving towards a chaotic state; a decrease in the fractal dimension indicates that events are gradually moving towards an ordered state. The calculation of fractal dimension is one of the core elements.

Grassberger and Procaccia proposed the G-P algorithm to compute the correlation dimension based on actual measured chaotic time series in 1983, which is now commonly applied to phase space reconstruction and correlation dimension calculation in one-dimensional space[43]. The AE ringing counts during four-point bending damage of RC beams can be considered as a one-dimensional time series $X = \{x_1, x_2, \cdots, x_n\}$. And after the determination of the embedded dimension m and the delay time τ, the phase space can be reconstructed as follows.

First, the original time series data,$\{x_1, x_2, \cdots, x_n\}$, are embedded by the m dimension, a subspace x_i of dimension m can be obtained by Eq. (2).

$$X_i = \left[x_i,\ x_{i+t} \ldots x_{i+(m-1)t}\right] i = 1, 2, \cdots, N_m \tag{2}$$

Obviously, the original time series will be reconstructed into N_m m-dimensions vectors. The reconstructed phase space is presented in Eq. (3).

$$X = \begin{bmatrix} x_1 & x_{1+\tau} & \cdots & x_{1+(m-2)\tau} & x_{1+(m-1)\tau} \\ x_2 & x_{2+\tau} & \cdots & x_{2+(m-2)\tau} & x_{2+(m-1)\tau} \\ \vdots & \vdots & \vdots & \vdots & \vdots \\ x_{N_m-1} & x_{N_m-1+\tau} & \cdots & x_{N-\tau+1} & x_{N-1} \\ x_{N_m} & x_{N_m+\tau} & \cdots & x_{N-\tau} & x_N \end{bmatrix} \tag{3}$$

The corresponding correlation function of these sub-vectors is defined as Eq. (4).

$$W(r(k)) = \frac{1}{{N_m}^2} \sum_{i=1}^{N_m} \sum_{j=1}^{N_m} H\left[r - ||X_i - X_j||\right] \tag{4}$$

Where N_m represents the number of time series data; H is the Heaviside step function, which can be presented in Eq. (5); The measurement scale, $r(k)$, of each point in the phase space can be calculated using Eq. (6); k represents the scaling coefficient.

$$H(u) = \begin{cases} 0, u < 0 \\ 1, u \geq 0 \end{cases} \tag{5}$$

$$r(k) = k \frac{1}{{N_m}^2} \sum_{i=1}^{N_m} \sum_{j=1}^{N_m} ||X_i - X_j|| \tag{6}$$

Given a scale $r(k)$, there is a corresponding correlation function $W(r(k))$ according to Eq. (4). Therefore, g scales could be obtained for g coordinate points. The resulting points are fitted using least-squares in the scale-free interval, and the correlation dimension D of the AE parameter sequence is the slope of the fitted line in accordance with Eq. (7).

$$D = -\lim_{\delta \to 0} \frac{\ln W(r(k))}{\ln r(k)} \tag{7}$$

3.2. Reconstructed phase space

The phase space reconstruction is a critical step in analyzing chaotic time series, and the determination of delay time τ and embedding dimension m is the key to the analysis, which will considerably impact the quality of the phase space after reconstruction. To determine the selection of the above two parameters, Kim et al. put forward an algorithm called the C-C method [44]. The C-C method considers that the delay time τ and the embedding dimension m are related to each other and cannot be selected separately from other traditional methods. The advantage of this algorithm makes it a widely used method in processing actual time series.

The core of the C-C method is to process the correlation integral for the embedded time series, and the correlation integral is calculated by Eq. (8) as follows:

$$C(m, N, r, \tau) = \frac{2}{N_m^2} \sum_{1 \leq i < j \leq N_m} H(r - \|x_i - x_j\|) \tag{8}$$

Where $H(a)$ is the Heaviside function, N is the number of the data set, N_m is the size of embedded points in m-dimensional space, and $\|\ldots\|$ denotes the sup-norm. $C(m, N, r, \tau)$ measures the fraction of the pairs of points $\{x_1, x_2, \cdots, x_n\}$, whose sup-norm separation is no greater than r.

The C-C method put forward a new dimensionless measure of nonlinear dependence as shown in Eq.(9).

$$S(m, N, r, \tau) = C(m, N, r, \tau) - C^m(1, N, r, \tau) \tag{9}$$

The remarkable feature of the statistic is that it is obtained by subtracting two correlation integrals, which is the reason why it is named the C-C algorithm. The existing statistical conclusions prove that this statistic can well quantify the sequence correlations of nonlinear time series. The delay time τ and the embedding dimension m are calculated by MATLAB.

3.2.1. Determination of the delay time τ

The C-C method is used to study the nonlinear dependence and eliminate incorrect temporal correlations. It divides the time original time series $\{x_1, x_2, \cdots, x_n\}$ into t disjoint time series. These disjoint time series are computed for $S(m, N, r, 1)$ as follows:

The single time series $\{x_1, x_2, \cdots, x_n\}$ corresponded to $t = 1$, and.

$$S(m, N, r, 1) = C(m, N, r, 1) - C^m(1, N, r, 1) \tag{10}$$

When$\tau = 2$, there are two disjoint time series $\{x_1, x_3, \cdots, x_{n-1}\}$ and $\{x_2, x_4, \cdots, x_n\}$ with the length $N/2$ respectively, and the $S(m, N, r, 2)$ is computed as Eq.(11):

$$\begin{aligned} S(m, N, r, 2) = \frac{1}{2}\{&[C_1(m, \frac{N}{2}, r, 2) - C_1^m(1, \frac{N}{2}, r, 2)] + [C_2(m, \frac{N}{2}, r, 2) \\ &- C_2^m(1, \frac{N}{2}, r, 2)] \end{aligned} \tag{11}$$

Similarly, for general τ, the format becomes:

$$S(m,N,r,\tau)=\frac{1}{\tau}\sum_{s=1}^{\tau}[C_s(m,\frac{N}{\tau},r,\tau)-C_s^m(1,\frac{N}{\tau},r,\tau)] \tag{12}$$

As $N\to\infty$, the formula above can be written as Eq.(13).

$$S(m,r,\tau)=\frac{1}{\tau}\sum_{s=1}^{\tau}[C_s(m,r,\tau)-C_s^m(1,r,\tau)],\quad m=2,3,\ldots \tag{13}$$

Ideally, $S(m,r,\tau)$ will keep equal to 0 for any r if the data are independently identically distributed when m and r are fixed. However, the data sets that exist in reality are finite and inevitably correlated. Thus the $S(m,r,\tau)$ calculated by real data sets won't be 0. Therefore, the times at which the zero crossing of $S(m,r,\tau)$ or $S(m,r,\tau)$ shows the least variation with r can be regarded as the optimal one. To further simplify the algorithm, several representative r_j are chosen and used to define the quantity in Eq(14).

$$\Delta S(m,t)=max\{S(m,r_j,\tau)\}-min\{S(m,r_j,\tau)\} \tag{14}$$

Which is used to measure the variation of $S(m,r,\tau)$ with r. Hence the locally optimal time τ can be determined by computing the minima of $\Delta S(m,\tau)$.

For a fix N, the data becomes sparser with the increase of m, which causes $C(m,N,r,\tau)$ to get smaller and smaller. Obviously, if r is too large, it will lead to the result that $C(m,N,r,\tau)$ get saturated, and approach to 1 cause most distances between point pairs are less than r. The existing statistical research and engineering practice results show that the reasonable value range of m is $2\sim7$, and it is recommended to set the range of r between $\sigma/2\sim2\sigma$, where σ is the standard deviation of the data set. The above preprocessing will make the subsequent calculation more convincing and efficient.

Further, $r_1=0.5\sigma$, $r_2=1.0\sigma$, $r_3=1.5\sigma$, $r_4=2.0\sigma$, are chosen to represent the variation of r. And the averages of the quantities are defined as Eq(15):

$$\Delta\overline{S}(\tau)=\frac{1}{6}\sum_{m=2}^{7}\Delta S(m,\tau) \tag{15}$$

And we look for the first occurrence of local minimum value of $\Delta\overline{S}(\tau)$, and regard it as the locally optimal time for the independence of the data.

Data collected from four beams are processed by C-C method to determine τ, the results are shown in Fig. 5. Basically, when $\tau=3$, The first minimum of ΔS(t) occurs. Therefore, $\tau=3$ is taken as the unified choice of delay time in the following analysis.

3.2.2. *Determination of the embedding dimension m*

Based on the above calculation method of correlation dimension D, a curve between D and the embedding dimension m can be drawn, as shown in Fig. 6. The selected m should ensure that the results are stable. It can be observed that although D changes with m, the "self-similarity" of the AE parameters will not be affected. Moreover, rather than the accurate numerical value, the change trend and change rules are more meaningful in this study. It can be seen that in Fig. 6, when the m is

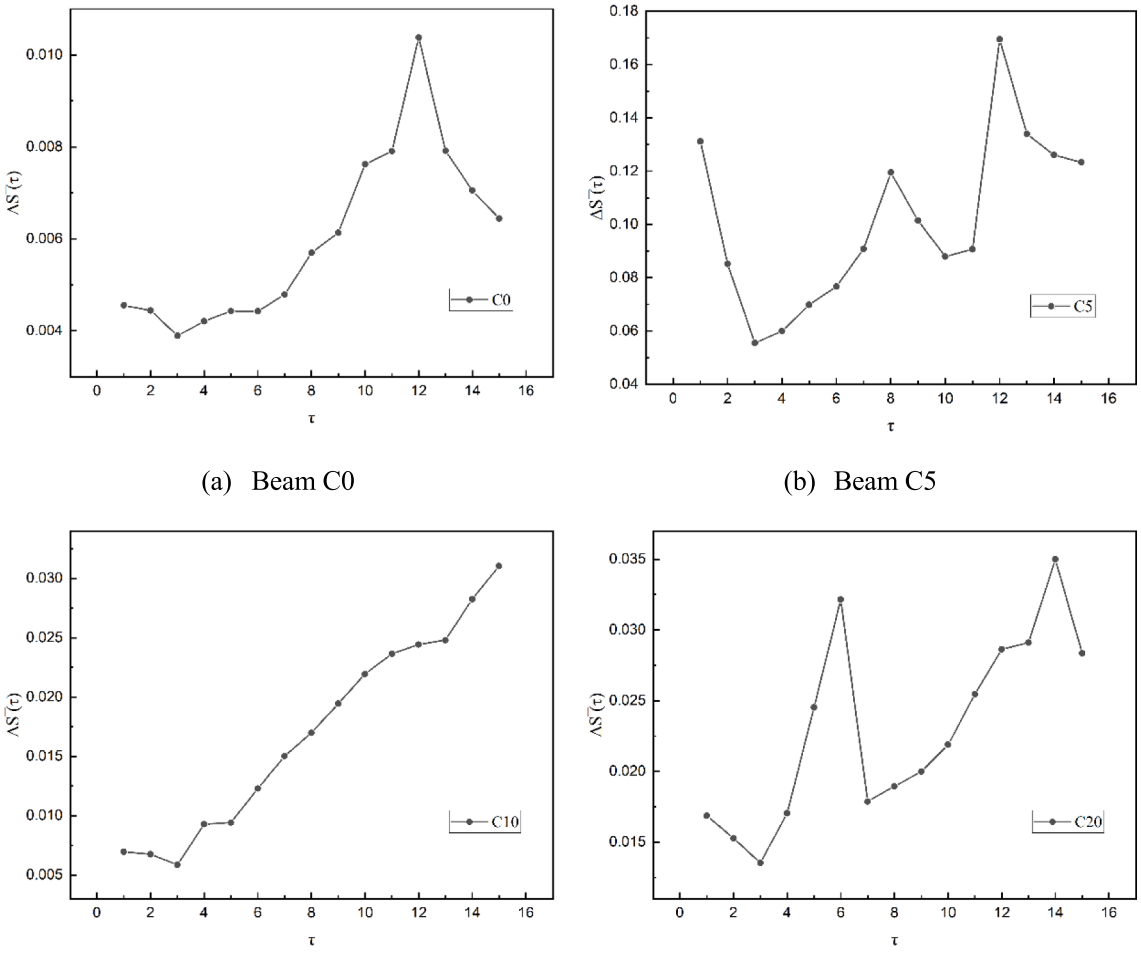

Fig. 5. $\tau-\Delta\overline{S}(\tau)$ relationship curves.

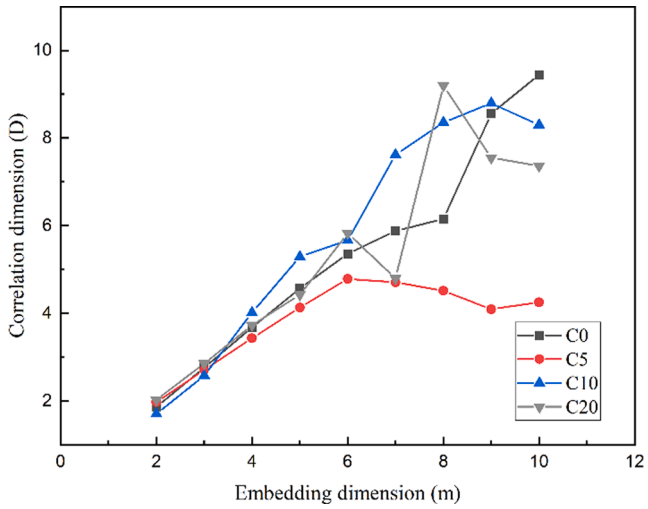

Fig. 6. Curve of correlation dimension *D* and the embedding dimension *m*.

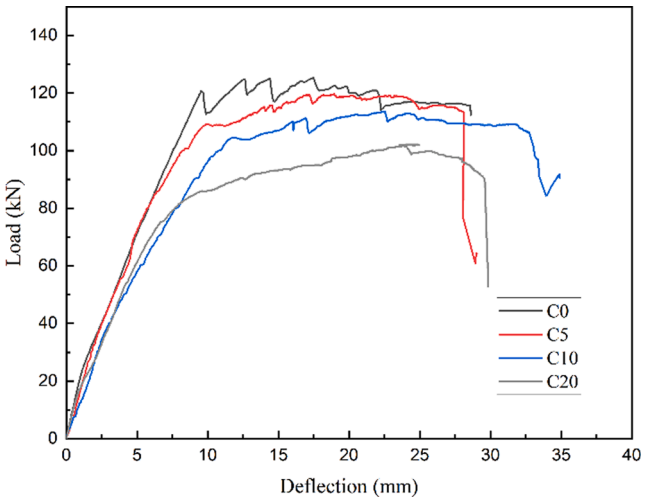

Fig. 7. The load–deflection curves of the tested beams.

between 3 and 5, the curve approaches a straight line, which means the gradient with the increase of the correlation dimension *D* tend to be stable. Thus, the embedding dimension *m* is set as 4.

4. Experimental results and discussions

4.1. Flexural behavior and damage patterns

The yield load, ultimate load, and the corresponding deflections for all the test beams are listed in Table 3. The flexure behavior of the tested beams is shown in Fig. 7. The ultimate loads of tested beams (C0, C5, C10, C20) are 125.3, 119.3, 111.3, and 102.6 kN, respectively. The deflection of all the specimens near the yielding of steel is found to be in the range of 2.47–5.12 mm. It was observed that the load capacity of beams gradually decreased with an increasing corrosion ratio. Typical failure patterns of beams C0, C5, C10, and C20 are shown in Fig. 8, respectively. In terms of uncorroded beam C0, slightly corroded beam C5, and moderate corroded beam C10, the failure occurred through yielding tensile bars followed by the crushing of concrete at the compression zone. Severely corroded beam C20 failed by yielding tensile bars followed by the removal of the concrete cover at the tension zone. This is because the corrosion of the reinforcement has led to a large number of corrosion cracks in the RC beams. And as the degree of corrosion rises, the bond performance between the reinforcement and concrete is greatly reduced.

4.2. AE ringing counts behavior

The AE ringing counts represent the total number of oscillations of the AE signals that exceed the threshold, which is often used to assess the activity of the AE signals and is easily influenced by the threshold [45]. Notable, although the AE ringing count detected from five sensors were slightly different in specific value, the overall trend was consistent[46]. This is attributed to AE technology has high sensitivity and the ability to detect damage in real time. Therefore, AE data from sensor 1 were used for analysis in this study. The AE ringing counts and cumulative AE ringing counts versus time for different corrosion degrees beams are shown in Fig. 9. It could be noted that the cumulative AE ringing counts decreased as the corrosion degree of the specimen increased. These results indicated that a higher corrosion level of reinforcement would cause more micro and macro cracks within the concrete, which will lead to a reduction in the net area of the fracture surface of the corroded beam and thus less space for crack development in the damage process. It coincided with the experimental observation.

Additionally, there is no obvious pattern of variation between the average ringing counts of single AE signal and reinforcement steel corrosion for tested beams, but rather shows fluctuations above and below a certain value. In the real experimental observation, once a large rupture in the concrete has been produced, there is a phased increase in AE ringing counts. Therefore, it could be concluded that larger AE ringing counts result from the release of energy during crack expansion and agglomeration and that there is a good correspondence between AE signals and concrete damage.

Table 3
Flexural behavior of the tested beams.

Beams	Yield Load	Ultimate Load	Yield Deflection	Ultimate Deflection
	kN	kN	mm	mm
C0	113.0	125.34	9.2	28.5
C5	105.0	119.3	8.4	28.1
C10	98.0	111.3	8.8	32.7
C20	83.5	102.6	8.0	29.5

4.3. Failure stage analysis of beams

Numerous research results have shown that AE ringing count is a characteristic parameter that can well reflect the variety of material properties because it is proportional to the strain energy released by the motion of dislocations and crack extension inside the material [9,47,48]. Therefore, AE ringing counts and cumulative ringing counts are used as parameters to represent the damage evolution of non-corroded and corroded beams.

Damage mechanics originated from the concept of continuity factor and effective stress proposed by Kachanov [49]. The damage index *ID* is as follows:

$$ID = 1 - \frac{A_e}{A_0} = \frac{A_d}{A} \tag{16}$$

$$A_0 = A_e + A_d \tag{17}$$

Where A_e is the effective area of the concrete; A_d is the area of concrete where the damage occurred; A is the initial area of the concrete. When $ID = 0$, it means that the material is entirely undamaged; as the load increases, A_d increases and A_e decreases; when $ID = 1$, it corresponds to complete damage.

It is assumed that N_m is the cumulative AE ringing counts when the entire section of the RC beams is destroyed; N_d represents the cumulative AE ringing counts when the damaged section area reaches A_d; Then, the damage index *ID* can be expressed as Eq. (18).

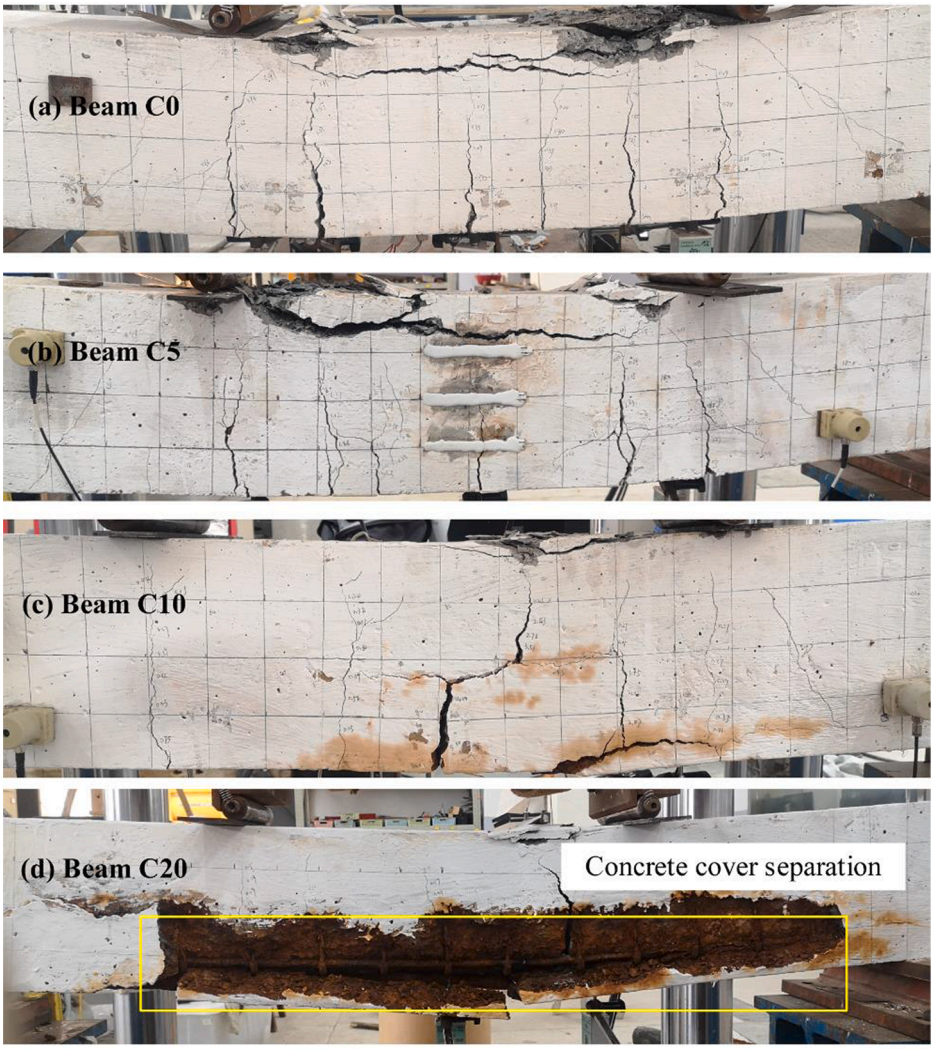

Fig. 8. Failure patterns of tested beams.

$$ID = \frac{N_d}{N_m} \tag{18}$$

Since the corrosion effect of the reinforcement will lead to the reduction of the bearing capacity of corroded RC beams, the initial damage caused by corrosion needs to be taken into account. ID_0 is determined by Eq. (19).

$$ID_0 = 1 - \frac{F_d}{F_0} \tag{19}$$

Where F_d represents the ultimate bearing capacity of the rusted beam, F_0 represents the ultimate bearing capacity of the uncorroded beam. Therefore, the modified damage index ID is shown in Eq. (20).

$$ID = ID_0 + (1 - ID_0)\frac{N_d}{N_m} \tag{20}$$

The relationship between the time and damage index for the RC beams with different corrosion rates is shown in Fig. 10. It can be seen that all four curves show an increasing trend. Besides, four points were marked on the damage index – time curves to indicate different damage situations of specimens. Specifically, Points A, B, D were determined by the tendency of cumulative AE ringing counts and the load–deflection of the tested RC beams, while the analysis of the fractal characteristics determined point C. Point A was the start point of AE ringing counts continued to grow rapidly; point B corresponded to the rebar yield; point C was the early-warning signal of critical transition for tested beams failure; point D corresponded to the failure of tested beams. Therefore, the damage process of the tested beams can be divided into three damage stages: the initial damage stage (i.e., before point A), the damage evolution stage (i.e., from point A to point B), and the continuous damage growth stage (i.e., point B to D), which was consistent with the results of other scholars in the four-point bending tests of non-corroded beams [50,51]. The accounting of AE signals and duration at different damage stages was provided in Table 4.

In the initial damage stage, there were few AE signals, and the AE ringing counts were at a low level. The duration of the first stage for tested beams C0, C5, C10, and C20 was relatively short, accounting for 18.5%, 11.5%, 12.7%, and 7.6% of the total loading process, respectively. Similarly, the AE ringing counts only accounted for 18.7%, 16.9%, 7.9%, and 3.1% of the cumulative AE ringing counts. Such behaviors indicated that the crack activity was weak and the damage was negligible at this stage. It was noted that as the corrosion level of reinforcement increases, the duration of the first stage (initial damage stage) becomes shorter. In terms of beams C0 and C5, a relatively large number of AE ringing counts appeared near point A, which was associated with the first occurrence of visible concrete cracks. For moderate corroded beam C10 and heavily corroded beam C20, visible cracks had existed on the concrete surface and it could thus be concluded that corrosion cracks within the concrete gradually closed under load, which exhibited less AE ringing count response and shorter duration.

At the damage evolution stage, a considerable number of AE ringing

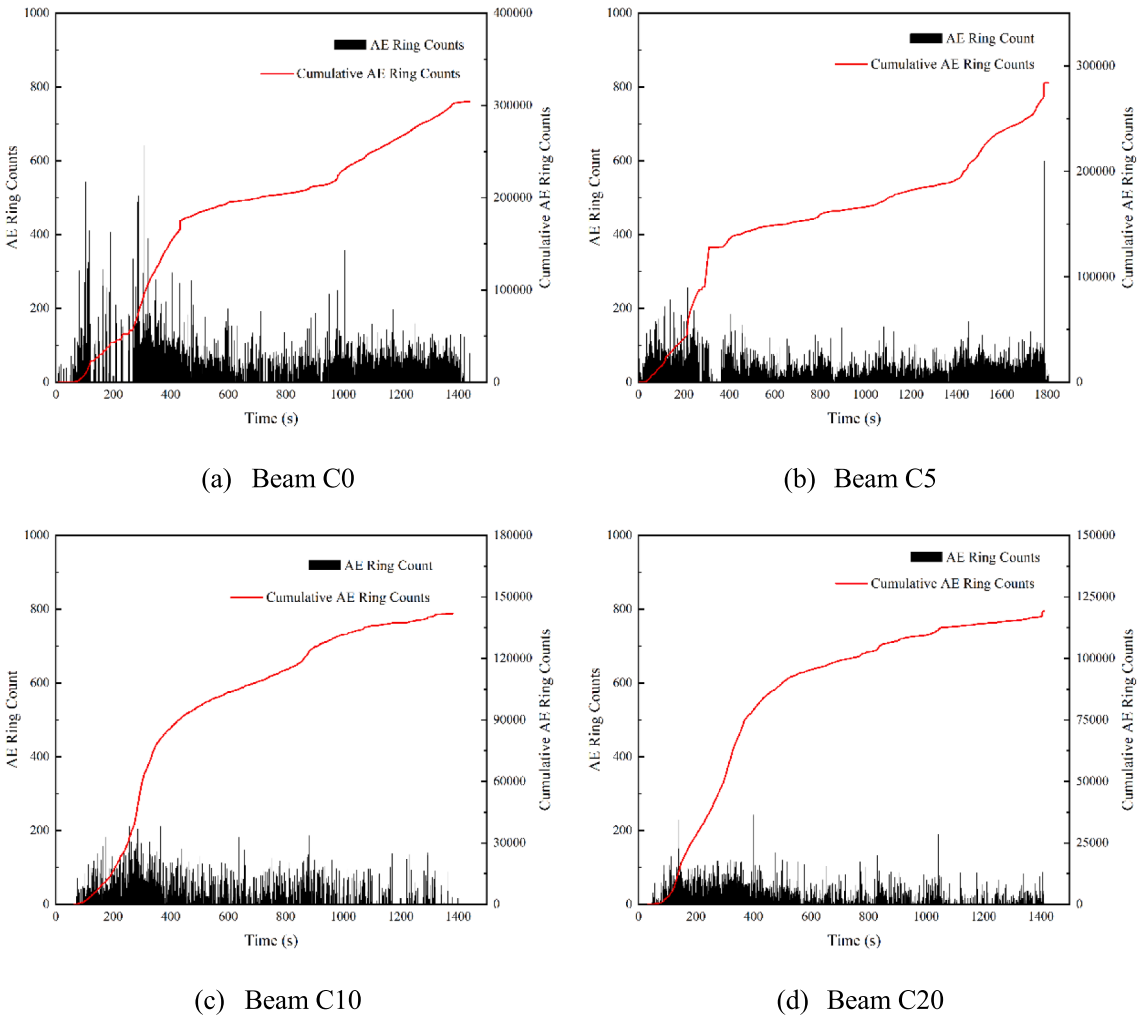

Fig. 9. Variation characteristics of AE ringing counts of tested beams with time.

counts were monitored, indicating the concrete cracking was in an active condition. In real experimental observation, macroscopic cracks had appeared and extended at the concrete surface, with a significant increase in response to AE ringing counts. As shown in Fig. 10, the damage index of tested beams increased approximately linearly at this stage.

At the continuous damage growth stage (i.e., from the beginning of steel yielding up to the final failure), AE signals growth slowed. It could be found that the duration of this stage is more prolonged, reaching 68.6% to 75.3% of the total duration. Remarkably, the third stage exhibited a higher proportion of AE ringing counts than the second stage for uncorroded beam C0 and slightly corroded beam C5, while it had a lower ratio of AE ringing counts than the second stage for moderate corroded beam C10 and severe corroded beam C20. This was because the lightly corroded and uncorroded beams produced more flexural cracks than the more severely corroded beams in the third stage. It indicated that the damage to the uncorroded and lightly corroded beams was mainly in the third stage, while the damage to the more severely (over 10%) corroded beams was concentrated primarily in the second stage.

4.4. Relationship between fractal dimension and damage index

Based on the C-C method, the damage index was divided into 20 groups on average from 0% to 100% (0%~5%,5%~10% and so on). And we used MATLAB to calculated the fractal dimension D of each group and determined whether the AE ringing count of specimens possessed fractal characteristics during the loading process. Fig. 11 shows several typical results of $\ln(r) - \ln(Wr)$ curves of tested beams. The minimum correlation coefficients R_{min} and the average correlation coefficient R_{av} for each beam are shown in Table 5. It could be observed that the average correlation coefficients R_{av} of each beam were greater than 0.99, while the minimum R_{min} of each beam are greater than 0.96, showing a significant correlation between the two parameters. This finding indicated that the AE parameter sequence in the failure process of the RC beams has self-similarity in the time domain.

Studies have shown that the AE events are mainly caused by the stress wave generated during the formation and development of the cracks in RC beams [52–54]. Thus, the fractal dimension D can be used as an indicator to describe the changes in mechanical properties and damage inside the RC beams. From a statistical point of view, the more disordered the data set is, the larger the fractal dimension is, corresponding to the actual situation that the generation and development of the direction and location of the microcracks are chaos. On the contrary, the more ordered the data set is, the smaller the fractal dimension is, reflecting the major large cracks continuously extending and widening in the RC beams. Fig. 12 showed the fractal dimension D - damage index relationships of RC beams with different corrosion ratios under four-point bending tests.

For uncorroded beam C0, in the initial damage stage, i.e., before reaching 20% damage degree, the fractal dimension D– damage curve exhibited a relatively large fluctuation (Fig. 12(a)). This was attributed

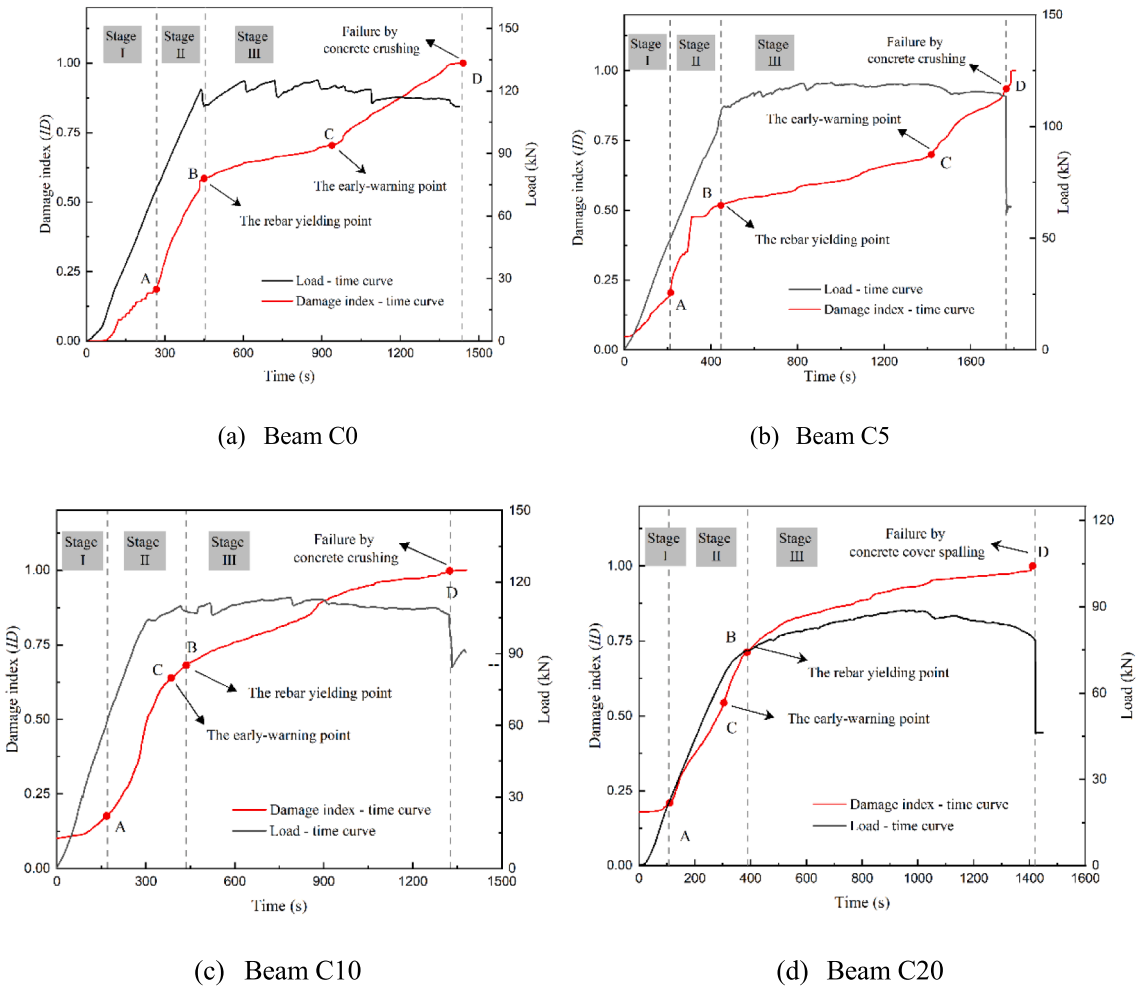

(a) Beam C0 (b) Beam C5

(c) Beam C10 (d) Beam C20

Fig. 10. Variation characteristics of damage index and a load of tested beams with time.

Table 4
The accounting of AE signals and duration at different loading stages.

Beams	The initial damage stage		The damage evolution stage		The continuous damage growth stage	
	Time percentage	AE ringing counts the percentage	Time percentage	AE ringing counts the percentage	Time percentage	AE ringing counts the percentage
C0	18.5%	18.7%	11.5%	38.3%	70.0%	43.0%
C5	11.5%	16.9%	12.2%	36.8%	75.3%	46.3%
C10	12.7%	7.9%	18.8%	56.0%	68.6%	36.1%
C20	7.6%	3.1%	18.8%	60.4%	73.6%	36.5%

to that internal crack evolution was mainly dominated by the closure of initial pores and mini-cracks, and its crack expansion had obvious disorderly. In the subsequent stage (which corresponds to the linear elastic stage), the fractal dimension D remained relatively stable in the range of 20%-45% damage degree, and then the D values increased from 3.64 to 4.36 in the range of 45%-65% damage degree. This finding indicated that many mini-cracks were randomly generated, and these mini-cracks gradually develop, expand and penetrate to form large-scale macro cracks. Moreover, the AE signal order gradually tended to weaken, and the self-similarity tended to decrease. Finally, in the continuous damage growth stage, the fractal dimension D slowly increased and reached the peak value of 4.64 when the damage degree reached 70%. Then, it dropped sharply and remained at a low value. This phenomenon indicated that the visible major large cracks of the beam were seriously and rapidly propagated at this stage, which showed a good correspondence with the real experimental observation.

As depicted in Fig. 12(b, c), the fractal dimension D - damage curves of RC beams C5 and C10 showed a similar variation trend. That is, in the initial damage stage, the fractal dimension curves of beams C5 and C10 fluctuated regularly and exhibited a slow downward trend, which is not the same as that of an uncorroded beam. It could be seen that the D values of beam C5 at a narrow interval of 3.16 to 3.76 before the damage index reached 45%, while those of beam C10 vary from 3.55 to 4.07. This was due to the presence of numerous corrosion cracks inside the RC beams, resulting in less disorderly sprouting of mini cracks and weaker self-similarity of AE signals. In the second stage, D values of beams C5 and C10 reached the minimum value first and then rose rapidly to the maximum. The obtained results showed minimal and maximal D values of 4.32 and 2.78, respectively, for beam C5, 4.28, and 2.98 for beam C10. This result presented that as the load increased, the bending cracks penetrated with the corrosion cracks and multiple fractures converged rapidly, leading to the disorderly expansion of many micro-cracks and the formation of large destructive primary cracks. Once the fractal dimension D values of C5 and C10 reached the maximum value, they

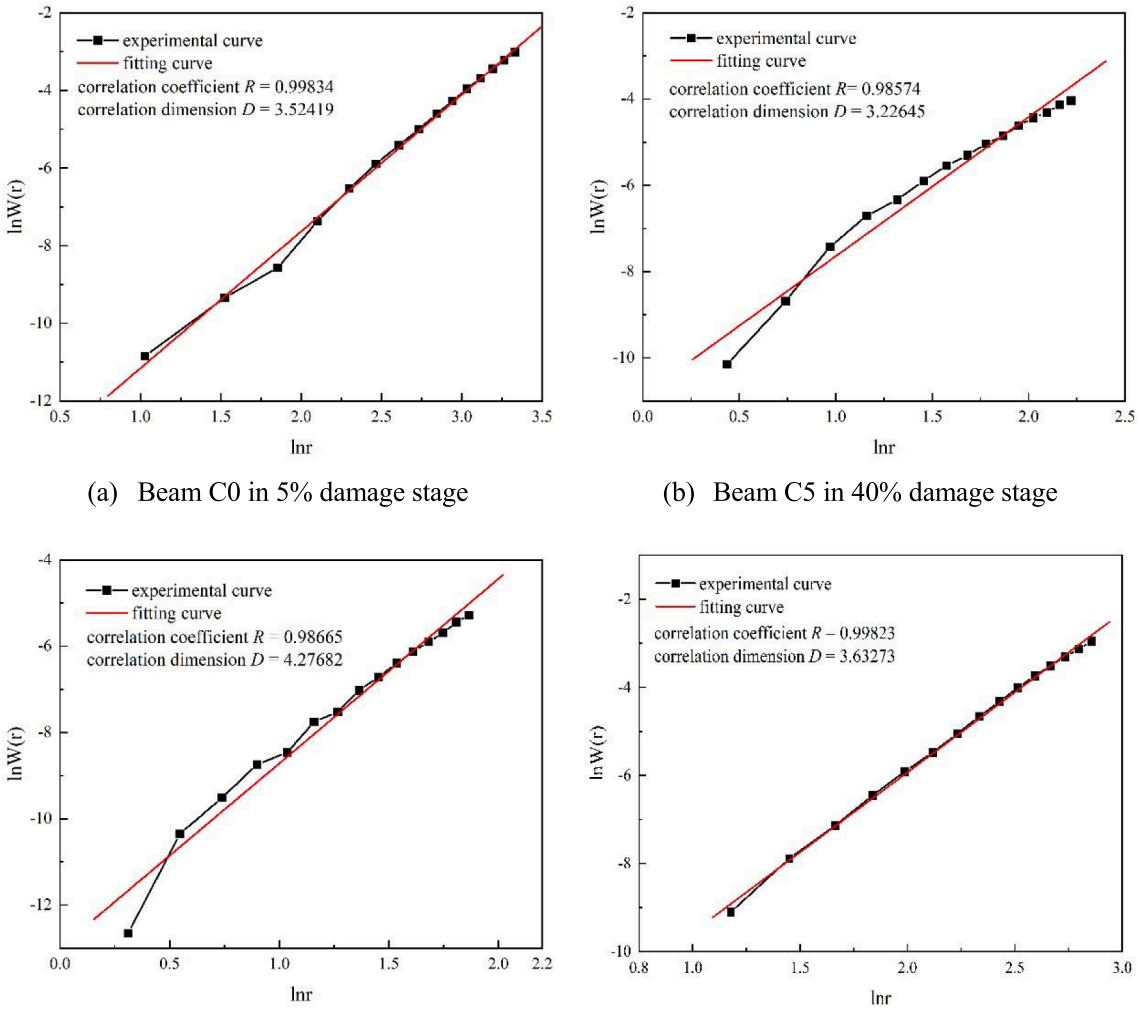

Fig. 11. Typical results of $\ln(r) - \ln(Wr)$ curves of tested beams.

Table 5
R_{min} and R_{av} for each beam.

Beams	C0	C5	C10	C20
R_{min}	0.986748	0.984212	0.964058	0.976307
R_{av}	0.996624	0.995954	0.994059	0.994965

exhibited a strong downward trend and reached the sub-minimum value when it utterly failed. This indicated that the AE signals of corroded RC beams changed from disordered to ordered. In the real experimental observation, several visible large-scale main cracks in the RC beams continue to develop and extend in different directions accompanied by the concrete crushing, resulting in the final destruction of corroded beams, which coincided with the results of the uncorroded beam C0.

As for the severe corroded beam C20, it could be observed that many visible corrosion cracks and the spalling of concrete cover. Furthermore, the fluctuation of fractal dimension in the whole process was more intense than for the other three beams. This illustrated that multiple scales of corrosion cracks were distributed in the interior of severely corroded beam C20. As the load increased, one portion of micro-cracks began to develop in a disorderly and scattered manner, and the other larger corrosion cracks extended along with the original orientation. Therefore, the correlation dimension of AE showed more drastic fluctuations. When the damage degree reached 55%, the correlation dimension D reached a maximum value of 4.54. Then D showed a stable downward trend as a whole with several localized low values in the process. During this stage, large-scale visible corrosion cracks on the surface of beam C20 develop rapidly, while micro-cracks continue to develop and accumulate into large-scale cracks simultaneously.

When the damage of the RC beams reached a certain degree, the fracture would lead to failure. It could be found that the fractal dimension of AE signals can precisely reflect the precursory information. As shown in Fig. 12, point C denoted the peak point of the fractal dimension D curves, and D-value decreased rapidly after point C until failure, indicating that the micro-cracks inside the RC beams rapidly merged into large visible cracks and the specimen was about to fail. Therefore, the peak point C could be defined as the early warning point of failure. The damage index at the warning points of the four test RC beams (C0, C5, C10, C20) were 70%, 65%, 65%, and 55%, respectively. It could be noted that the damage index corresponding to the peak point decreases with the increase of corrosion degree. The peak, corresponding to the experimental phenomenon, means the major destructive cracks are about to appear, and the early appearance of peak value might be explained by the fact that due to the corrosion effect of the steel reinforcement leads to a decrease in the load-carrying capacity of the RC beams, its ductility is weakened, and the degree of brittleness is increased. This conclusion was coinciding with the practical engineering needs. Although the warning points occurred before the yielding points

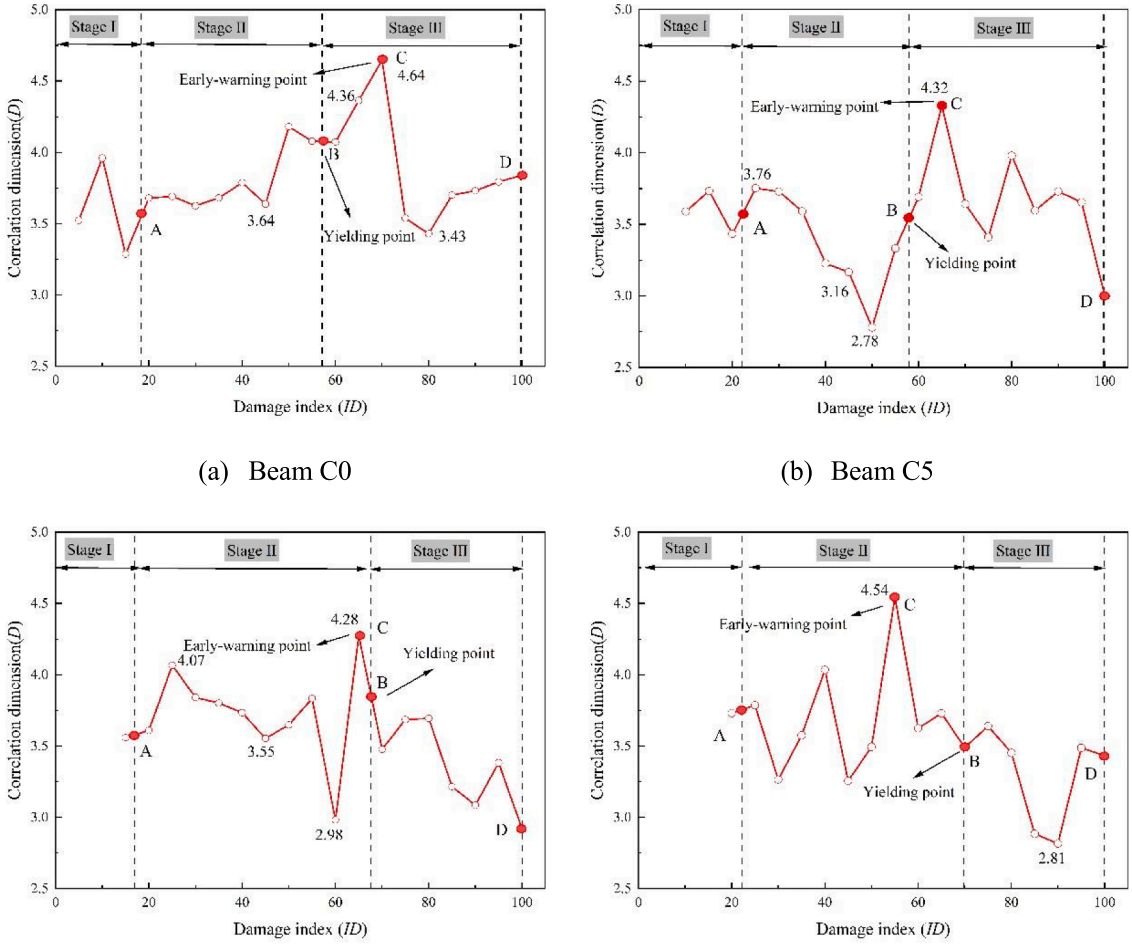

Fig. 12. Fractal dimension – damage index curves of tested beams.

in RC beams C10 and C20, it corresponds to the phenomenon that the initial corrosion of C10 and C20 has made the concrete cover on the surface of tensile reinforcement cracks obviously, even spalling. The higher the degree of corrosion, the earlier the warning; this feature makes it valuable in practical engineering applications. Furthermore, the fractal dimension with AE monitoring for early warning of instability is applicable and practical.

5. Conclusion

The present study investigated the correlation between damage evolution information and AE data using fractal theory methods and G-P algorithms to study crack evolution in RC beams with different corrosion degrees under the bending test. The study indicated that AE fractal dimension analysis could effectively reflect the whole stage's crack magnitude and development, which have an important value for enriching the early warning of failure in corroded RC beams. The primary conclusions are listed below.

(1) The yield load and ultimate load of corroded beams gradually decreased with the increase of corrosion degree. Beams C0, C5 and C10 failed by failed by yielding tensile bars followed by the crushing of concrete at compression zone. In terms of severely corroded beam C20, it failed by yielding tensile bars followed by removing the concrete cover at tension zone.

(2) AE ringing counts analysis revealed that there is a good correspondence between AE signals and concrete damage, and the damage process of the specimens could be divided into three damage stages: the initial damage stage (I), the damage evolution stage (II), the continuous damage growth stage (III). Besides, the damage to the uncorroded and lightly corroded beams (C0, C5) was mainly in the third stage, while the damage to the moderate and severely corroded beams (C10, C20) was concentrated primarily in the second stage.

(3) Based on the acoustic emission rate process theory and the effect of corrosion, a damage evolution model of RC beams at different corrosion rates was developed. It could be used to monitor the internal damage of RC beams under different corrosion rates and quantitatively assess the damage level during the fracture process.

(4) The AE ringing counts of the corroded and uncorroded beams during the failure process had obvious fractal characteristics. The fractal dimension analysis could effectively reflect the development of crack magnitude and crack pattern in the whole stage. This work can clearly investigate the differences in crack evolution between RC beams with different corrosion degrees.

(5) There are significant similarities in corroded and uncorroded beams' fractal dimension fluctuation laws under four-point bending. When the damage of the RC beams reached a certain extent, *D*-value showed a fluctuating rise to a peak and then a sharp drop before damage. The damage corresponding to the peak point would move forward with the increase of corrosion degree. This result accurately

reflects the precursory information and provides an early warning point for the failure of corroded RC beams.

CRediT authorship contribution statement

Yonglai Zheng: Supervision, Funding acquisition. **Yuan Wen:** Methodology, Investigation, Writing – original draft. **Tanbo Pan:** Conceptualization, Methodology, Investigation, Writing – review & editing. **Yongcheng Liu:** Methodology, Investigation. **Yujue Zhou:** Resources, Funding acquisition. **Ruizhi Li:** Writing – review & editing. **Yubao Zhou:** Supervision.

Declaration of Competing Interest

The authors declare that they have no known competing financial interests or personal relationships that could have appeared to influence the work reported in this paper.

Acknowledgements

The authors are grateful for the financial support from the Natural Science Foundation of Fujian Province, China (Grant Nos. 2022 J011185), Education Department of Fujian Province and Provincial Key Laboratory of Construction Materials & Structural Reinforcement, Sanming University, Sanming, China.

References

[1] C.Q. Fang, K. Lundgren, L.G. Chen, C.Y. Zhu, Corrosion influence on bond in reinforced concrete, Cem. Concr. Res. 34 (2004) 2159–2167.
[2] E. Chen, C.K.Y. Leung, A coupled diffusion-mechanical model with boundary element method to predict concrete cover cracking due to steel corrosion, Corros. Sci. 126 (2017) 180–196.
[3] J. Alam, L.A.C. Neves, H. Zhang, D. Dias-da-Costa, Assessment of remaining service life of deteriorated concrete bridges under imprecise probabilistic information, Mech. Syst. Sig. Process. 167 (2022).
[4] J. Bressan, F. Ghrib, A. El Ragaby, FRCM Strengthening of Corrosion-Damaged RC Beams Subjected to Monotonic and Cyclic Loading, J. Compos. Constr. 26 (2022).
[5] F.J. Tang, G.S. Zhou, H.N. Li, E. Verstrynge, A review on fiber optic sensors for rebar corrosion monitoring in RC structures, Constr. Build. Mater. 313 (2021).
[6] K. Andisheh, A. Scott, A. Palermo, Experimental evaluation of the residual compression strength and ultimate strain of chloride corrosion-induced damaged concrete, Struct. Concrete 20 (2019) 296–306.
[7] F. Jnaid, R.S. Aboutaha, Residual flexural strength of corroded reinforced concrete beams, Eng. Struct. 119 (2016) 198–216.
[8] Y.L. Zheng, Y.J. Zhou, Y.B. Zhou, T.B. Pan, L.M. Sun, D. Liu, Localized corrosion induced damage monitoring of large-scale RC piles using acoustic emission technique in the marine environment, Constr. Build. Mater. 243 (2020).
[9] Y.Q. Wu, S.L. Li, D.W. Wang, G.H. Zhao, Damage monitoring of masonry structure under in-situ uniaxial compression test using acoustic emission parameters, Constr. Build. Mater. 215 (2019) 812–822.
[10] J.G. Yue, Y.N. Wang, D.E. Beskos, Uniaxial tension damage mechanics of steel fiber reinforced concrete using acoustic emission and machine learning crack mode classification, Cement Concrete Comp. 123 (2021).
[11] P.R. Prem, M. Verma, A.R. Murthy, P.S. Ambily, Smart monitoring of strengthened beams made of ultrahigh performance concrete using integrated and nonintegrated acoustic emission approach, Struct. Control Hlth. 28 (2021).
[12] N. Reboul, C. Grazide, N. Roy, E. Ferrier, Acoustic emission monitoring of reinforced concrete wall-slab connections, Constr. Build Mater. 259 (2020).
[13] D.G. Aggelis, T. Shiotani, S. Momoki, A. Hirama, Acoustic emission and ultrasound for damage characterization of concrete elements, Aci. Mater. J. 106 (2009) 509–514.
[14] Q.Q. Zheng, Y. Xu, H. Hu, J.W. Qian, Y. Ma, X. Gao, Quantitative damage, fracture mechanism and velocity structure tomography of sandstone under uniaxial load based on acoustic emission monitoring technology, Constr. Build Mater. 272 (2021).
[15] M. El-Tahan, A. Hassanein, W.A. Megid, K. Galal, Evaluation of Reinforced Concrete T-Beams Retrofitted in Shear with Mechanically Anchored Dry Carbon Fiber Sheets, Exp. Tech. 46 (2022) 647–660.
[16] X.H. Zhou, W.C. Shan, J.P. Liu, J. Li, Fracture characterization of composite slabs with different connections based on acoustic emission parameters, Struct. Control & Health Monitoring 28 (2021).
[17] J.M.C. Ongpeng, A.W.C. Oreta, S. Hirose, Damage progression in concrete using acoustic emission test through convex hull visualization, ACI Mater. J. 113 (2016) 737–744.
[18] A.A. Abouhussien, A.A.A. Hassan, Acoustic emission-based analysis of bond behavior of corroded reinforcement in existing concrete structures, Struct. Control Hlth 24 (2017).
[19] M. Abdelrahman, M.K. ElBatanouny, P.H. Ziehl, Acoustic emission based damage assessment method for prestressed concrete structures: modified index of damage, Eng. Struct. 60 (2014) 258–264.
[20] S. Garhwal, S. Sharma, S.K. Sharma, Acoustic emission monitoring of RC beams corroded to different levels under flexural loading, Arab J. Sci. Eng. 46 (2021) 4319–4335.
[21] Y. Kawasaki, S. Wasada, T. Okamoto, K. Izuno, Evaluation for RC specimen damaged from rebar corrosion by acoustic emission technique, Constr. Build Mater. 67 (2014) 157–164.
[22] K. Zhang, X.H. Liu, W.L. Liu, S. Zhang, Influence of weak inclusions on the fracturing and fractal behavior of a jointed rock mass containing an opening: experimental and numerical studies, Comput. Geotech. 132 (2021).
[23] R. Zhang, J. Liu, Z.Y. Sa, Z.Q. Wang, S.Q. Lu, C.F. Wang, Experimental investigation on multi-fractal characteristics of acoustic emission of coal samples subjected to true triaxial loading-unloading, Fractals 28 (2020).
[24] Z.Q. Jia, H.P. Xie, R. Zhang, C.B. Li, M. Wang, M.Z. Gao, Z.P. Zhang, Z.T. Zhang, Acoustic emission characteristics and damage evolution of coal at different depths under triaxial compression, Rock Mech. Rock Eng. 53 (2020) 2063–2076.
[25] A. Lisjak, Q. Liu, Q. Zhao, O.K. Mahabadi, G. Grasselli, Numerical simulation of acoustic emission in brittle rocks by two-dimensional finite-discrete element analysis, Geophys. J. Int. 195 (2013) 423–443.
[26] Z.B. Zhang, E.Y. Wang, N. Li, Fractal characteristics of acoustic emission events based on single-link cluster method during uniaxial loading of rock, Chaos Soliton Fract 104 (2017) 298–306.
[27] B.B. Mandelbrot, Citation Classic - the Variation of Certain Speculative Prices, Current Contents/Social & Behavioral Sciences, (1982) 20-20.
[28] E. Garcia-Ochoa, F. Corvo, Copper patina corrosion evaluation by means of fractal geometry using electrochemical noise (EN) and image analysis, Electrochem. Commun. 12 (2010) 826–830.
[29] R. Lopes, P. Dubois, I. Bhouri, H. Akkari-Bettaieb, S. Maouche, N. Betrouni, Fractal geometry for medical signal analysis: a review, Irbm 31 (2010) 189–208.
[30] R. Lopes, N. Betrouni, Fractal and multifractal analysis: a review, Med. Image Anal. 13 (2009) 634–649.
[31] E. Zha, R. Zhang, Z.T. Zhang, T. Ai, L. Ren, Z.P. Zhang, Y. Liu, C.D. Lou, Acoustic emission characteristics and damage evolution of rock under different loading modes, Energies 13 (2020).
[32] K. Zhao, X. Yu, S.T. Zhu, Y.J. Yan, Y. Zhou, Z.W. He, Y.F. Song, M. Huang, Acoustic emission fractal characteristics and mechanical damage mechanism of cemented paste backfill prepared with tantalum niobium mine tailings, Constr. Build Mater. 258 (2020).
[33] H. Sun, X.L. Liu, J.B. Zhu, Correlational fractal characterisation of stress and acoustic emission during coal and rock failure under multilevel dynamic loading, Int. J. Rock Mech. Min. 117 (2019) 1–10.
[34] J. Liu, Y. Yang, J. Xie, Y. Liu, Acoustic emission test and damage fractal characteristics analysis of concrete with different initial porosity, Trans. Beijing Institute of Technol. 38 (2018) 1231–1236.
[35] C. Wu, Q. Shi, F. Yang, Experimental study on fractal dimension of acoustic emissions on the damage to reinforced concrete, J. Disaster Prevention and Mitigation Eng. 36 (2016) 895.
[36] Y.S. Wang, J. Liu, Fractal analysis of damage detected by acoustic emissions in prestressed reinforced concrete beam under loading, Aer. Adv. Eng. Res. 30 (2016) 295–299.
[37] Y. Wang, C. Yan, T. Zhang, N. Wang, L.J. Chen, G. Jie, Acoustic emission fractal characteristics analysis of steel fiber reinforced concrete during uniaxial tensile damage, Mater. Testing 62 (2020) 329–336.
[38] A.A. Abouhussien, A.A.A. Hassan, acoustic emission monitoring of corrosion damage propagation in large-scale reinforced concrete beams, J. Perform. Constr. Facil 32 (2018).
[39] T.A. El Maaddawy, K.A. Soudki, Effectiveness of impressed current technique to simulate corrosion of steel reinforcement in concrete, J. Mater. Civ. Eng. 15 (2003) 41–47.
[40] P.R. Prem, A.R. Murthy, Acoustic emission and flexural behaviour of RC beams strengthened with UHPC overlay, Constr. Build Mater. 123 (2016) 481–492.
[41] F. Liu, R. Guo, X.J. Lin, X.F. Zhang, S.F. Huang, F. Yang, X. Cheng, Monitoring the damage evolution of reinforced concrete during tunnel boring machine hoisting by acoustic emission, Constr. Build. Mater. 327 (2022).
[42] M.N. Noorsuhada, An overview on fatigue damage assessment of reinforced concrete structures with the aid of acoustic emission technique, Constr. Build. Mater. 112 (2016) 424–439.
[43] P. Grassberger, I. Procaccia, Estimation of the Kolmogorov-Entropy from a Chaotic Signal, Phys. Rev. A 28 (1983) 2591–2593.
[44] H.S. Kim, R. Eykholt, J.D. Salas, Nonlinear dynamics, delay times, and embedding windows, Physica. D 127 (1999) 48–60.
[45] C. Chen, X.Q. Fan, X.D. Chen, Experimental investigation of concrete fracture behavior with different loading rates based on acoustic emission, Constr. Build. Mater. 237 (2020).
[46] S.L. Li, L.G. Zhang, P. Guo, P. Zhang, C. Wang, W.C. Sun, S.L. Han, Characteristic analysis of acoustic emission monitoring parameters for crack propagation in UHPC-NC composite beam under bending test, Constr. Build. Mater. 278 (2021).
[47] F.Z. Du, S.S. Pan, D.S. Li, Damage evaluation and failure mechanism analysis of steel tube confined reinforced-concrete columns by acoustic emission technology, Lat. Am. J. Solids Stru. 15 (2018).

[48] T.J. Zhang, Z.Q. Ling, M.K. Pang, Y.K. Meng, Experimental study of creep acoustic emission characteristics of coal bodies around boreholes under different moisture contents, Energies 14 (2021).
[49] D.R. Hayhurst, P.R. Dimmer, M.W. Chernuka, Estimates of Creep-Rupture Lifetime of Structures Using Finite-Element Method, J. Mech. Phys. Solids 23 (1975) 335–1000.
[50] W. Dong, J.B. Ye, Y. Murakami, H. Oshita, S. Suzuki, T. Tsutsumi, Residual load capacity of corroded reinforced concrete beam undergoing bond failure, Eng. Struct. 127 (2016) 159–171.
[51] T.V. Fursa, M.V. Petrov, D.D. Dann, A Method for Evaluating Failure in Reinforced Concrete under Bending Based on the Response of Electrical Parameters to an Impact Action, Russ. J. Nondestruct+ 54 (2018) 519–527.
[52] S.M. Liu, X.L. Li, Z.H. Li, P. Chen, X.L. Yang, Y.J. Liu, Energy distribution and fractal characterization of acoustic emission (AE) during coal deformation and fracturing, Measurement 136 (2019) 122–131.
[53] G. Ma, H. Li, Acoustic emission monitoring and damage assessment of FRP-strengthened reinforced concrete columns under cyclic loading, Constr. Build. Mater. 144 (2017) 86–98.
[54] G. Birck, I. Iturrioz, G. Lacidogna, A. Carpinteri, Damage process in heterogeneous materials analyzed by a lattice model simulation, Eng. Fail. Anal. 70 (2016) 157–176.